Accuracy Quantification of the Loci-CHEM Code for Chamber Wall Heat Fluxes in a GO_2/GH_2 Single Element Injector Model Problem

Jeff West, Doug Westra, Jeff Lin and Kevin Tucker
National Aeronautics and Space Administration
Marshall Space Flight Center
Huntsville, AL 35812

A robust rocket engine combustor design and development process must include tools which can accurately predict the multi-dimensional thermal environments imposed on solid surfaces by the hot combustion products. Currently, empirical methods used in the design process are typically one dimensional and do not adequately account for the heat flux rise rate in the near-injector region of the chamber. Computational Fluid Dynamics holds promise to meet the design tool requirement, but requires accuracy quantification, or validation, before it can be confidently applied in the design process.

This effort presents the beginning of such a validation process for the Loci-CHEM CFD code. The model problem examined here is a gaseous oxygen (GO2)/gaseous hydrogen (GH2) shear coaxial single element injector operating at a chamber pressure of 5.42 MPa. The GO2/GH2 propellant combination in this geometry represents one the simplest rocket model problems and is thus foundational to subsequent validation efforts for more complex injectors.

Multiple steady state solutions have been produced with Loci-CHEM employing different hybrid grids and two-equation turbulence models. Iterative convergence for each solution is demonstrated via mass conservation, flow variable monitoring at discrete flow field locations as a function of solution iteration and overall residual performance. A baseline hybrid grid was used and then locally refined to demonstrate grid convergence. Solutions were also obtained with three variations of the k-omega turbulence model.

Background

Design of reliable and durable combustion devices will be a key element in achieving the NASA Vision for Space Exploration. This analysis effort in the injector/chamber thermal compatibility area focuses on validating Computational Fluid Dynamics (CFD) tools for injector and chamber design by demonstrating accuracy levels for prediction of injector-generated thermal environments in the combustion chamber.

Almost 50 years of experience has proven that injector/combustor failures are typically the result of locally severe environments and, thus, multi-dimensional. As an example, note the severe injector-induced blanching and cracking in a main combustion chamber wall as shown in Figure 1. Given what are sure to be aggressive schedules and tight budgets for Space Exploration engine development, new injector design tools are needed to help reduce both the development time and cost of the combustion devices. Combustor thermal environments are a direct consequence of injector design and operation. Current injector design tools are mostly one-dimensional and empirical. The design tool shortcomings force either component over-design or an extensive, costly test

program to reveal and fix serious design issues. Accurate, efficient tools are essential for the design of robust combustion devices hardware.

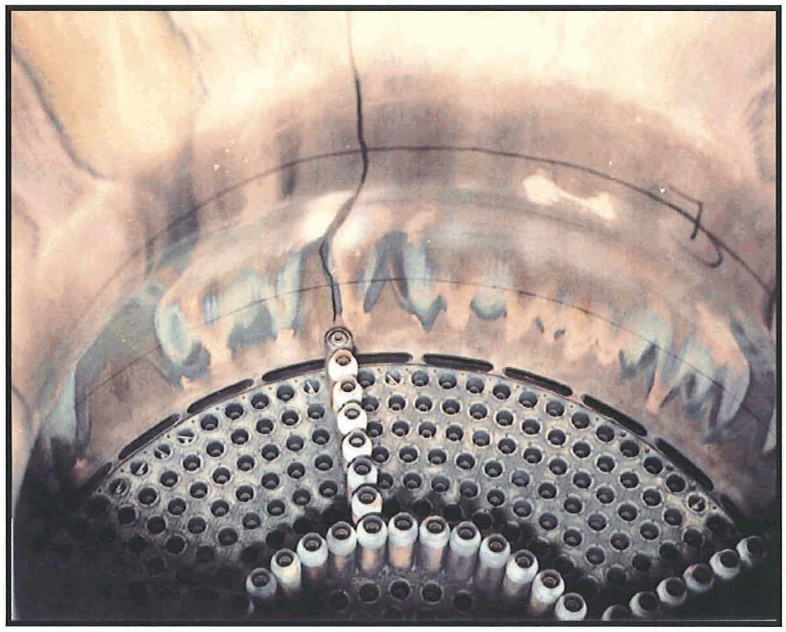

Figure 1. Blanching and cracking—evidence of multi-dimensional environments in a combustion chamber.

CFD holds great, but to date, largely unfulfilled promise for predicting the complex, three-dimensional environments during the design cycle time frame. Currently, injector designers continue to use their legacy tools despite the well-known issues associated with their use. They correctly point out that the CFD solutions are too time-consuming and are of questionable accuracy. The realization of CFD's promise as an injector design tools will require the demonstrated improvement in the three design tool requirements: simulation fidelity in terms of physics, boundary conditions and geometry; simulation robustness in terms of ability to produce solutions in the design cycle time frame; and simulation accuracy in terms of comparison to relevant data.

The combustion CFD technology effort at NASA/Marshall Space Flight Center is guided by a Combustion Devices CFD Simulation Capability Roadmap[1]. The Roadmap objective is to enable the use of CFD as a tool for the Simulation of Preburners, Ducting, Thrust Chamber Assemblies and Supporting Infrastructure in terms of Performance, Life, and Stability so as to affect the design process in a timely fashion.

If CFD is to be used as an injector design tool, code developers & code users must address the following key issue. How should confidence (i.e. demonstrated accuracy capability) in simulations and modeling for design be critically addressed, and where necessary, improved? Verification and Validation of computational solutions are the primary means to quantify and build this confidence.

The definitions[2] of Verification and Validation as applied to CFD analysis bear repeating. Verification is the process of determining that a model implementation accurately represents the developer's conceptual description of the model and the solution to the model. Significant verification efforts[3] for the CFD tool applied in this effort are underway. Verification will not be further addressed in this paper. Validation is

the process of determining the degree to which a model is an accurate representation of the real world from the perspective of the intended uses of the model. The last three phrases of the validation definition imply that an accuracy requirement has been defined. In this paper no accuracy requirement will be defined; our goal is only to determine the degree of accuracy.

Scope

The scope of this effort is limited to the simulation and evaluation of the results of modeling the RCM-1 test case titled "Penn State Preburner Combustor". The details of this test case is described in other documentation and will not be described further here unless the explanation of the modeling approach demands otherwise.

The specific goals of this effort are a) to achieve steady state solutions and demonstrate iteration and grid convergence and b) to compare the results of the chamber wall heat flux with experimentally determined values and provide a detailed critique of the comparison. In the accomplishments of these goals we will consider the effects of different turbulence models and of preconditioning and different hybrid grid strategies.

Computational Tools

Loci-CHEM is a finite-volume flow solver for generalized grids developed at Mississippi State University supported in part by NASA and NSF. Loci-CHEM uses high resolution approximate Riemann solvers to solve finite-rate chemically reacting viscous turbulent flows. Preconditioning[4] is available for low Mach number applications. Various chemical reaction mechanisms are available; the model used in this study for hydrogen/oxygen is a 6 species 28 reaction model[5] as shown in Table 1. Thermodynamic properties are provided via a standard partition function formulation which calculates the specific heats, internal energies and entropies of each individual perfect gas species. Several turbulence models are available; the Mentor Shear Stress Transport[6] (SST) and original Wilcox[7] k-omega models were used in the current study. Details of the numerical formulation are presented in the Loci-CHEM user guide.[8] Loci-CHEM is comprised entirely of C and C++ code and is supported on all popular UNIX variants and compilers. Parallelism is supplied by the Loci[9] framework which exploits multi-threaded and MPI libraries to provide parallel capability.

Table 1. The six-species hydrogen oxygen reaction model. Units are mks. $k_f=AT^n e^{(-E/RT)}$, k_r determined from Kc.

Step	Reaction	A	N	E/R (K)
Non M-body Reactions				
1	H2O + O <-> 2 OH	$5.8x10^{10}$	0	9059
2	H2O + H <-> OH + H2	$8.4x10^{10}$	0	10116
3	O2 + H <-> OH + O	$2.2x10^{11}$	0	8455
4	H2+O <-> OH + H	$7.5x10^{10}$	0	5586
M-body Reactions				
5	H2 + M <-> 2 H + M	$5.5x10^{15}$	-1	51987
6	O2 + M <-> 2 O + M	$7.2x10^{15}$	-1	59340
7	H2O + M <-> OH + H + M	$5.2x10^{18}$	-1.5	59386
8	OH + M <-> O + H + M	$8.5x10^{15}$	-1	50830

All grids are generated using GRIDGEN from Pointwise Corporation.[10] Hybrid grids were generated by extruding connecters representing the axi-symmetric solid surfaces normal to the solid surface into the computational domain with an initial defined spacing and stretch rate. The extrusion was terminated at the location where the extruded cells possessed an aspect ratio of approximately unity. This allowed a good quality transition from structured to unstructured cell types. The remainder of the computational domain was gridded using unstructured cells with a boundary decay factor of approximately 0.995 to avoid radical coarsening of the unstructured grid.

Computational Model

A sketch showing the boundary conditions for all eight cases is shown in Figure 2. The inlet walls and post-tip are adiabatic, no-slip walls. The oxygen and hydrogen inlets are both modeled as a fixed mass flow rate. Inlet boundary values for turbulence quantities, k and omega, were specified as $5x10^{-6}$ m^2/s^2 and 500 1/s respectively. While these values are lower than those recommended[6], the turbulent field develops in the injector inlets and previous experience has shown that the injector inlet distances in this case allow no sensitivity of the chamber solution to the injector inlet turbulence quantities specification. The temperature profile specified in the RCM-1 case definition document is imposed as a boundary condition on the no-slip chamber wall.

The faceplate and nozzle wall temperature boundary conditions are set as isothermal fixed temperatures with no-slip conditions for the flow. The faceplate was set to the value of the first data point, 639 K, from Table 3 of the RCM-1 case definition document. The nozzle wall temperature was set to the value of the last data point, 510 K.

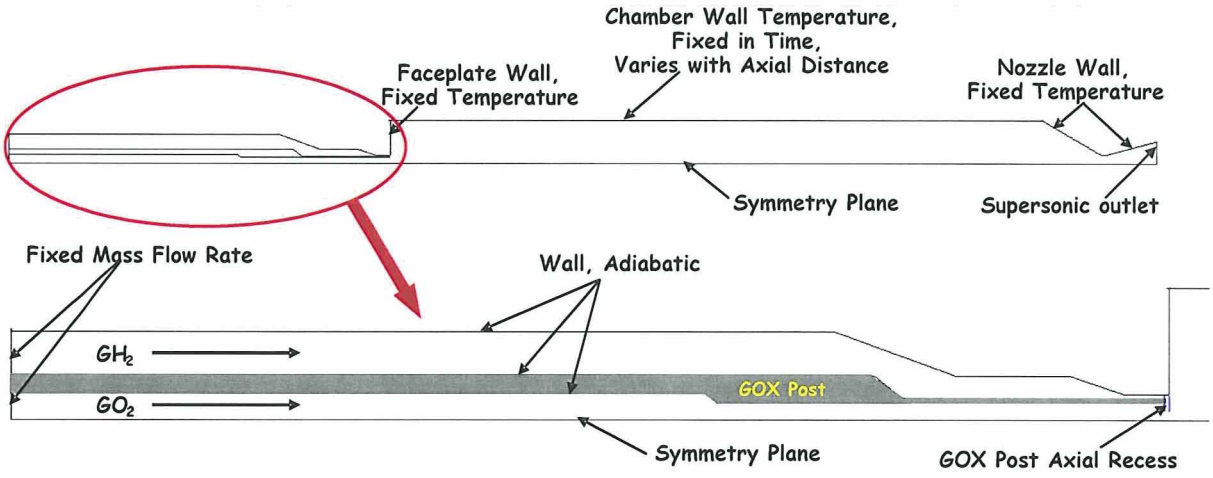

Figure 2. Sketch of the computational domain indicting location and type of boundary conditions.

The computational domain was initialized to quiescent steam at 780 K and 750 psia to start the steady state simulation. The steam provided a high enough initial temperature, such that when the reactant streams reached the post-tip region and mixed, self-ignition occurred. Loci-CHEM was executed in local time stepping mode with a physical time step of $1x10^{-4}$ seconds which was dynamically reduced locally to not exceed a maximum CFL number of 10,000 or a change in temperature, pressure or density variables of more than 10 percent. With these settings, these cases ignited relatively smoothly, i.e., the ignition did not cause any sustained reverse flow of propellants into either the fuel or oxidizer inlet tubes.

Solution convergence is evaluated by a combination of residual drop, total mass flow convergence in terms of integrated mass at inlet verses integrated mass at outlet, species stored mass convergence integrated over the entire domain volume, and temperature and pressure iteration history at selected probe point locations throughout the flow-field. In addition the chamber wall heat flux was monitored as a function of solution iteration until convergence was identified. For the cases presented in this paper three orders of magnitude of residual drop are obtained. This is less than observed in other CFD programs due to the use of the local time stepping feature documented above in which the time step increases as the solution converges, thus tending to increase residuals.

Computational domain mass conservation was always achieved to with 0.1 percent of the total mass flow. Global mass conservation does not necessarily mean that the mass of the individual species is not changing with time or iteration. For example, hydrogen and oxygen could be forming into water in some part of the chamber without any net change in global mass flow rate. Therefore, we track species conservation by integrating the stored mass of each individual species within the entire modeled domain and tracking that integrated value versus iteration. The species stored masses are also driven down to less than 0.1 percent of the total stored mass of that species. Similarly, the probe point pressures and temperatures are also driven down to less than 0.1 percent variation.

A typical solution requires about 10,000 time steps to achieve steady state convergence. For a 500,000 cell grid, using 16 AMD Opteron 246 processors, steady state convergence requires approximately 4 days of wall clock time or 1,600 cpu hours.

As long as the number of cells per processor remains similar to that described above, the Loci-CHEM CFD program is nearly perfectly scalable. Computer resources required for other grids used in this study can be scaled accordingly.

A sample flow field result in shown in Figure 3 for the baseline case. The oxidizer has mixed and combusted in the first half of the chamber length. The recirculation in the forward end of the chamber extends to about one-third of the chamber length. As illustrated in Figure 4, the recirculation is composed of a majority of water vapor and a minority of hydrogen on a mass basis.

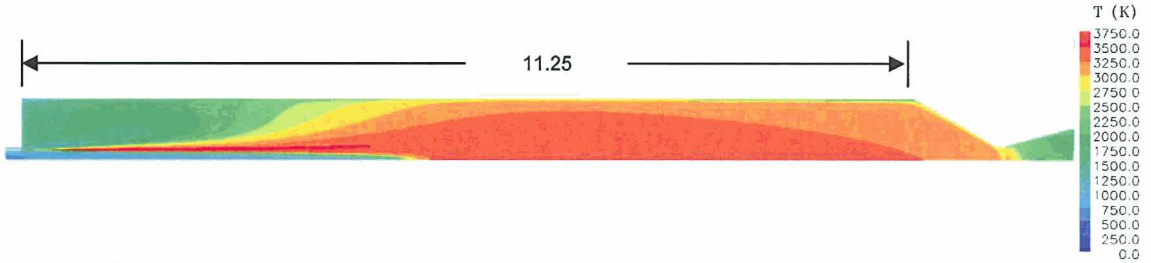

Figure 3. Computed temperature distribution, in degrees K, for the baseline case, Grid 2.

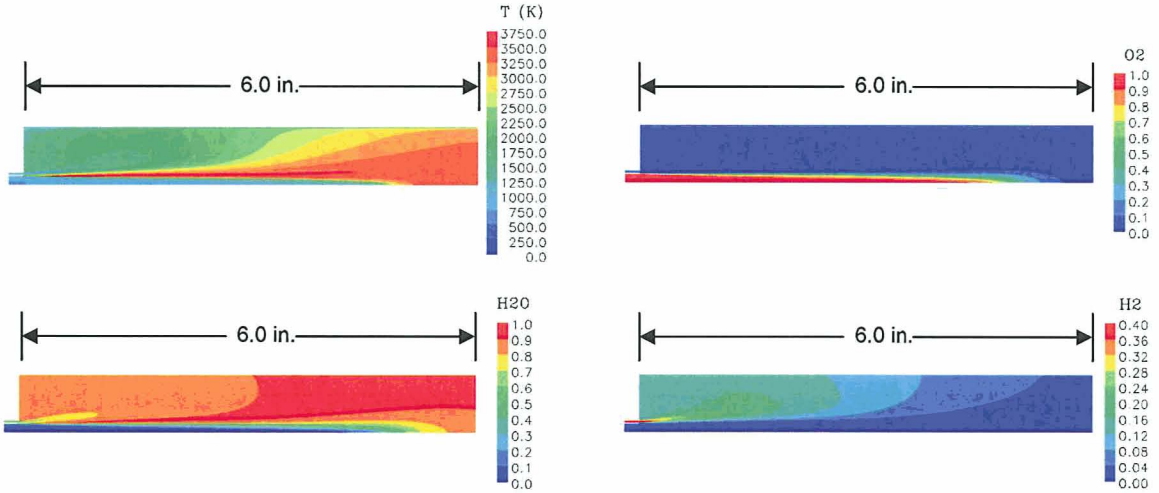

Figure 4. Close-up views of the temperature, oxygen, water vapor and hydrogen mass fraction distributions of the baseline case flow field, Grid 2.

Results

As mentioned above, the effects of turbulence model selection, preconditioning and grid convergence will be assessed for their impact on the predicted chamber wall heat flux. The grids used in the study are described first.

Grid Refinement Studies

A total of eight different axisymmetric grids were used to assess grid convergence, hereafter referred to as Grid 1 through 8. Grid 1 was generated as part of an earlier study[11] and consists of 51,030 structured grid cells. The grid spacing along the chamber wall is approximately 1×10^{-4} inches which corresponds to a first cell y-plus

value of approximately 1.3. Due to the limitations of structured gridding techniques, the first cell y-plus values for other solid surfaces were much greater than unity and resulted in unsatisfactory resolution of the turbulent boundary layer. Attempts to resolve all boundary layers to a y-plus value of unity resulted in very large cell counts, very large cell aspect ratios, and high concentration of cells in locations of little variable gradient. Therefore, all subsequent grids were of the hybrid type. Details of Grid 1 are shown in Figure 5.

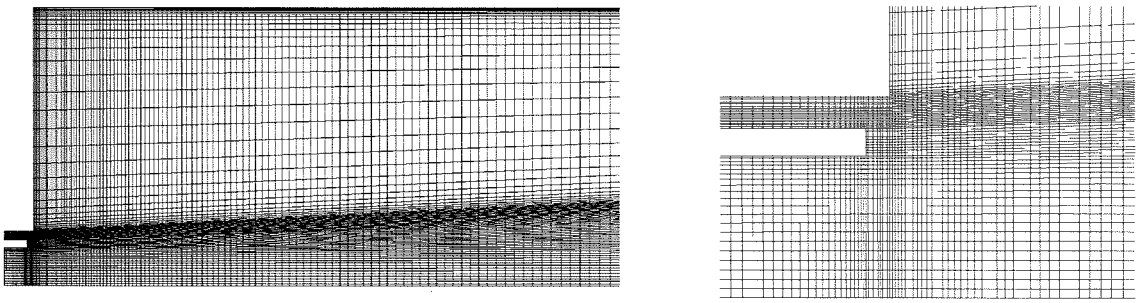

Figure 5. Details of Grid 1

Realizing the structured grid limitations, we decided to use a hybrid grid approach. In this approach the turbulent boundary layer is resolved on a structured grid grown hyperbolically from the solid surface to the estimated outer edge of the turbulent boundary layer. The remainder of the computational domain volume is discretized with unstructured cells. In this manner the gridding requirements of the turbulence model can be satisfied along all solid-surface boundaries.

The first, baseline hybrid grid was generated with an estimate of appropriate resolution of both the turbulent boundary layers and the non-boundary–layer regions of the computational domain. Grid 2 achieves first cell y-plus values ranging from 0.1 to 0.75 for all solid surfaces except the converging-diverging nozzle, where it ranges from 0.5 to 3.3. The extrusion stretch rate is nominally 1.2 for the structured layer of cells. The unstructured potion of the grid is constructed of triangular cells with sides ranging from 3×10^{-4} to 1.8×10^{-2} inches. The total number of cells used to construct Grid 2 is 496,496. Details of Grid 2 are shown in Figure 6.

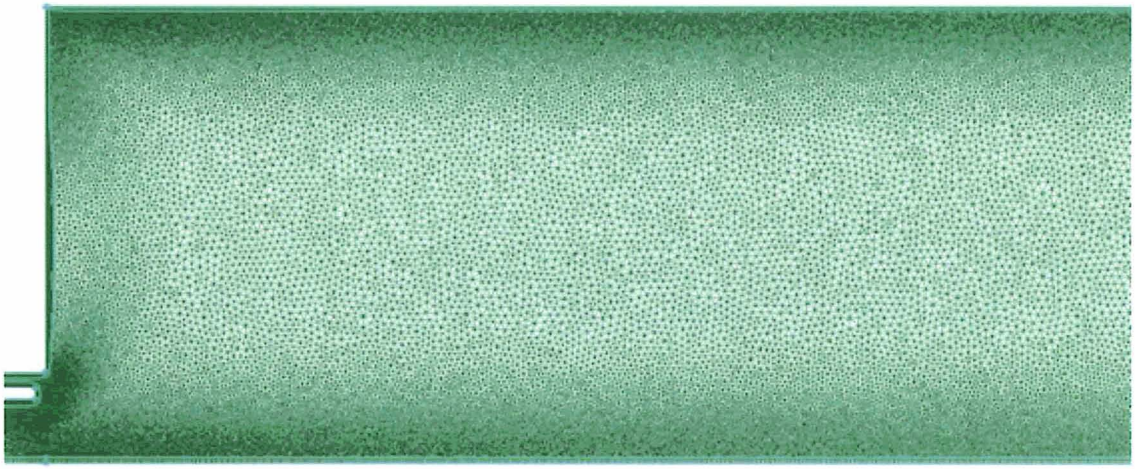

Figure 6. Details of Grid 2.

We addressed the grid refinement of the non-boundary layer region and the boundary layer region separately. First, we reduced the maximum triangular cell side length from 1.8×10^{-2} to 9.0×10^{-3} inches in the non-boundary layer portion of the grid. The resulting grid, Grid 3, was constructed of a total of 743,936 cells. Details of the head end of the chamber of Grid 3 are shown in Figure 7. Comparison with Grid 2 in Figure 6 shows the refinement of the chamber region as a result of the change.

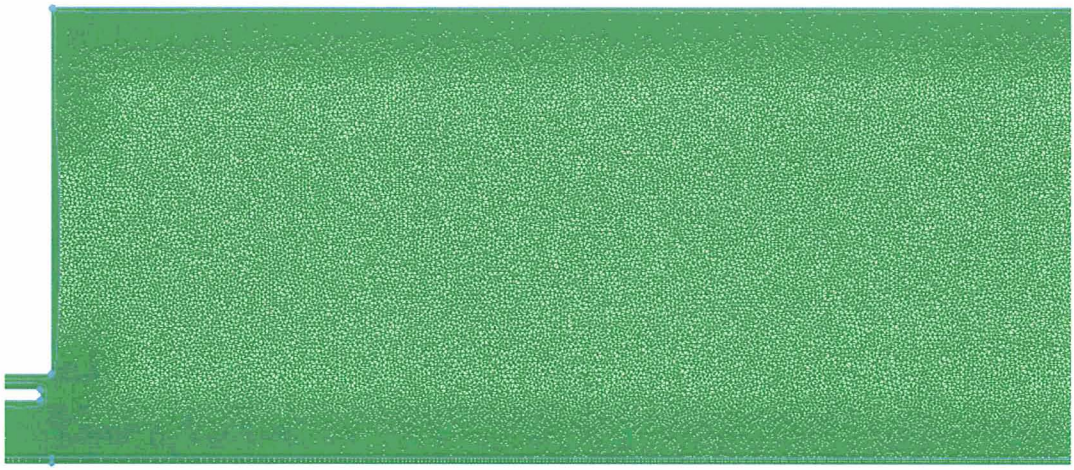

Figure 7. Details of Grid 3.

Then we created a sub-region in which the upstream half of the flame is located. We specified the maximum triangular cell side length in this sub-region as 6.2×10^{-3} inches. The properties for the main unstructured region were unchanged form those used in Grid 2. This new grid, Grid 4 was constructed of 782,872 cells.

We then combined the specifications of the unstructured regions from Grid 3 and Grid 4 and created Grid 5, which is constructed of 993,848 cells. A comparison between

Grid 2 and Grid 5 is contained in Figure 8. The refinement in the flame sub-region results in a factor of three better spatial resolutions than Grid 2.

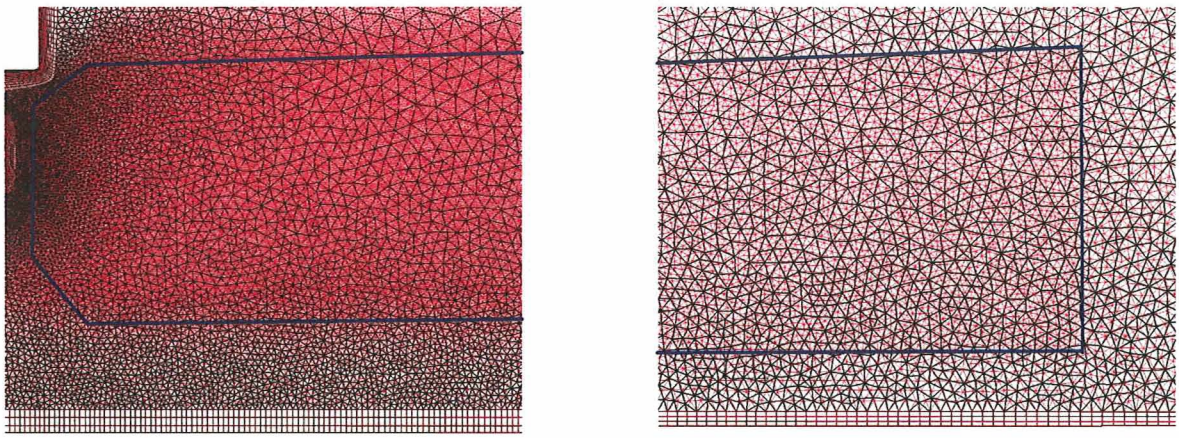

Figure 8. Comparison of Grid 2 (black) and Grid 5(red) in the near post tip region and the downstream region.

Next, we addressed the grid refinement of the boundary layer region. There are three quantities that can be readily changed in a structured extruded grid. They are initial spacing normal to the wall, the growth or stretch rate as the cells are extruded from the solid boundary and the cell spacing parallel to the solid wall.

The stretch rate was reduced from 1.2 in Grid 2 to 1.1 for Grid 6 while holding the initial cell spacing nearly constant. Grid 7 increases the initial cell spacing while retaining the stretch rate of 1.1. Grid 8 reduces the initial cell spacing both parallel and normal to the chamber wall relative to Grid 2 while retaining the stretch rate of 1.1. See Figures 9 and 10 for a summary of the main characteristics of the chamber wall boundary layer grides used in the grid sensitivity evaluation.

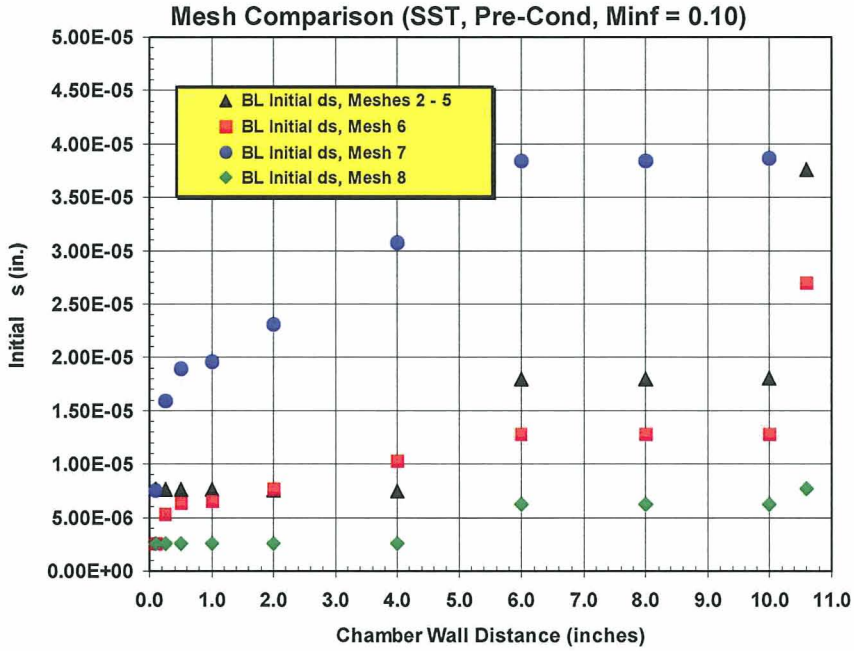

Figure 9 Variation of grid initial spacing normal to the chamber wall for all hybrid grides.

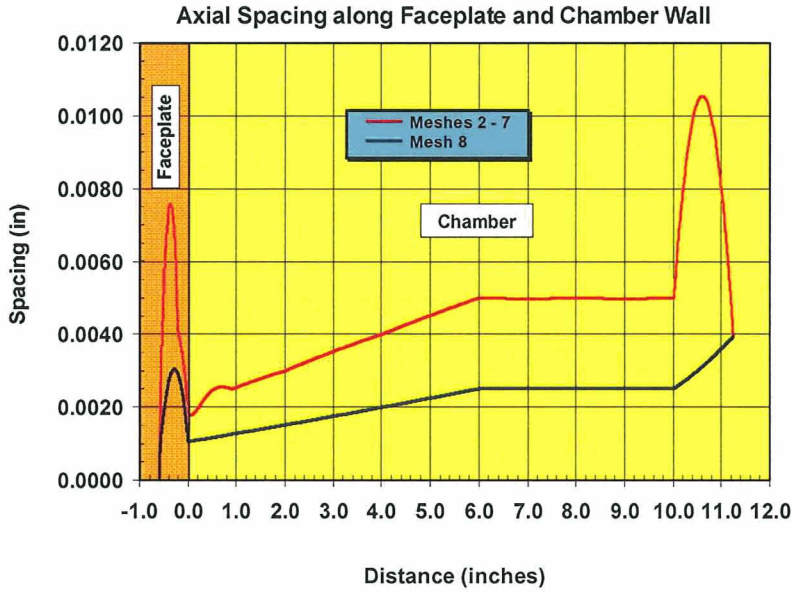

Figure 10. Variation of grid initial spacing parallel to the chamber wall for all hybrid grides as a function of perimeter distance from the injector outer diameter corner.

Computational Results

NASA/MSFC has been studying this RCM-1 case for some time. In 2004, an initial study[11] was conducted using Grid 1 with a previous version of the Loci-CHEM CFD program. Although the inlet and boundary conditions are not precisely those of the RCM-1 definition, they were a good approximation of the RCM-1 case. The predicted

heat flux compared to the experimentally determined heat flux is shown in Figure 11. The Mentor Baseline and Shear Stress Transport models are a better qualitative and quantitative representation of the experimentally determined heat fluxes than the Wilcox model. They both indicate the first heat flux peak is the largest magnitude.

This comparison was repeated using the hybrid structured-unstructured Grid 2 and the results are shown in Figure 12. A similar result is obtained with a slight quantitative advantage when using the SST model. This perceived advantage is based on the desire that a computational prediction to support design must be capable of predicting the location and magnitude of the greatest threat environments. The heat flux rise rate is important also, but the Wilcox model, which better predicts the rise rate does not do well on predicting the peak heat flux details. All models equally over-predict the heat flux downstream of the 5 inch location.

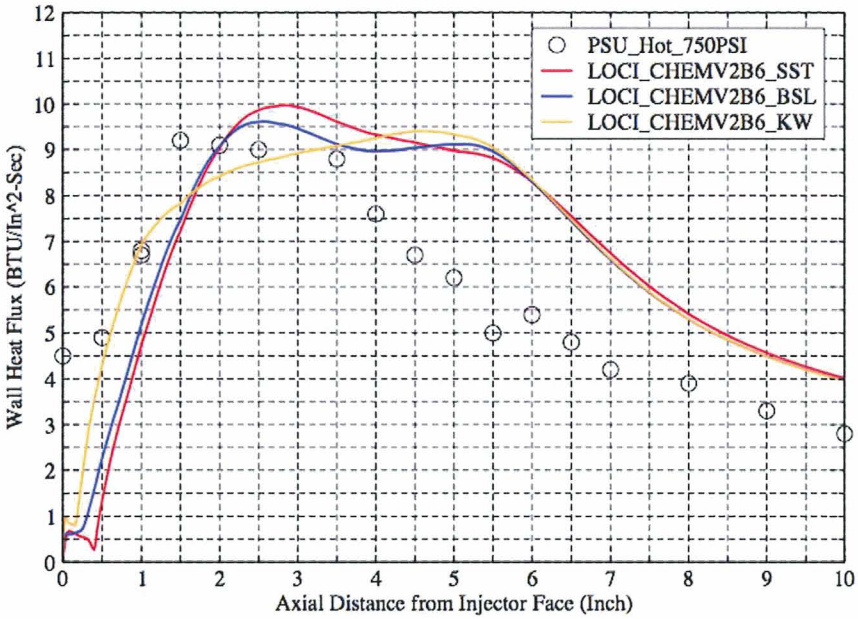

Figure 11. Comparison of heat flux computed with three different turbulence models in Loci-CHEM version 2 to the experimentally determined value.

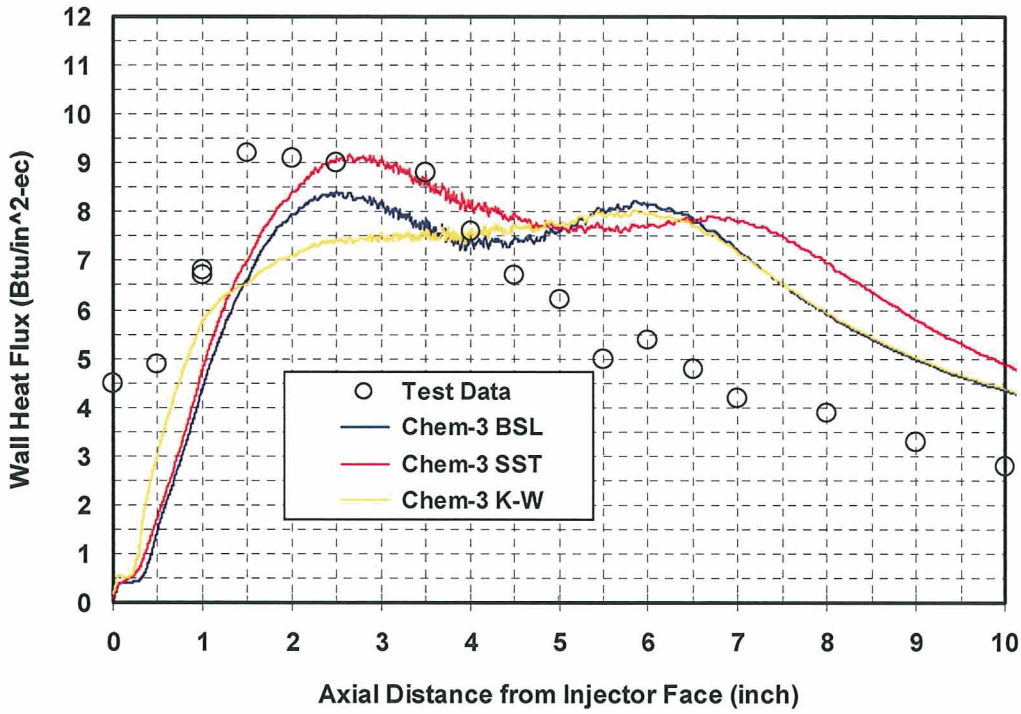

Figure 12. Comparison of heat flux computed with three different turbulence models to the experimentally determined value.

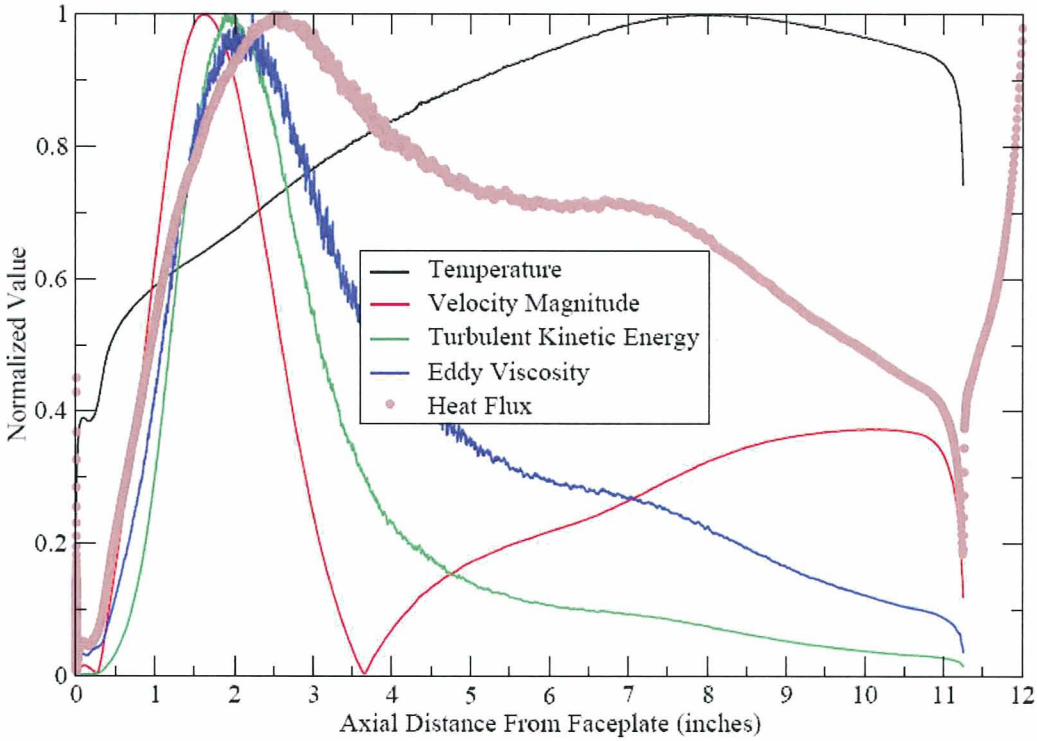

Figure 13. Profiles of normalized chamber near wall values for Grid 2.

Some discussion of the predicted dual peak nature of the heat flux profile is in order. Experimental data does not clearly indicate a dual peak of the heat flux profile. To gain some insight into the predicted nature, normalized values of predicted temperature, velocity magnitude, turbulent kinetic energy, eddy viscosity and heat flux as a function of distance from the faceplate at a radial-location of 0.74 inches, i.e., 0.1 inches form the chamber wall are shown in Figure 13. The heat flux peaks at about 2.5 inches downstream of the faceplate. The injector flow attaches to the wall downstream of this location at about 3.65 inches downstream of the faceplate as indicated by the velocity magnitude disappearing. The velocity magnitude, turbulent kinetic energy and eddy viscosity all peak upstream of the heat flux peak. The gas-phase temperature continues to rise throughout the first two-thirds of the chamber. The reductions in three of the four variables influencing the evolution of the heat flux downstream of about 2 inches cause the heat flux to reduce in the downstream direction after its first peak. After the flow attachment location, the velocity magnitude outside of the boundary layer increases while the turbulent kinetic energy and eddy viscosity continue to decrease slowly. This enables a second rise in the heat flux due to increased convective heat transfer. This rise is terminated by the plateau of the external boundary gas-phase temperature and the continued drop in turbulent kinetic energy and eddy viscosity, which results in a second peak in the predicted heat flux profile.

Next, the effect of preconditioning on the predicted heat flux was assessed using Grid 2 and the SST turbulence model. The Loci-CHEM implementation of preconditioning requires the specification of a global mach number scale, M_∞. Experience has shown that reasonable accuracy can be obtained for Mach number down to about 10 percent of this value. We inspected the flow field computed using Grid 2 and consequently set the M_∞ to 0.1, which allows good resolution down to a Mach number of about 0.01. The effect of preconditioning on the predicted heat flux is shown in Figure 14. Although the activation of preconditioning caused no significant change in the predicted heat flux, its use did significantly increase the efficiency of obtaining convergence. Due to this result, all subsequent computations were executed using preconditioning and all figures in this paper using the description baseline are those computed using preconditioning.

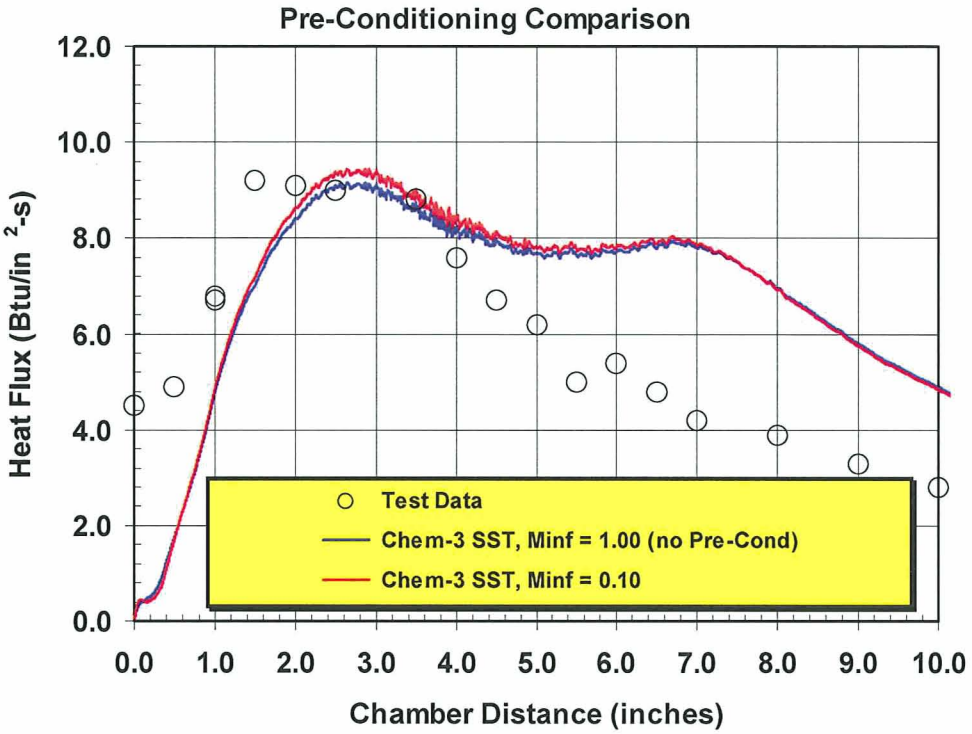

Figure 14. Effect of preconditioning on predicted heat flux for the parameter value of M_∞ of 0.1.

To asses the effects of grid convergence, predicted heat fluxes using Grids 2 through 5 are compared in Figure 15. These non-boundary layer region refinements systematically decrease the heat flux by approximately five percent in the upstream portion of the chamber and increase the heat flux by a similar amount in the downstream portion of the chamber.

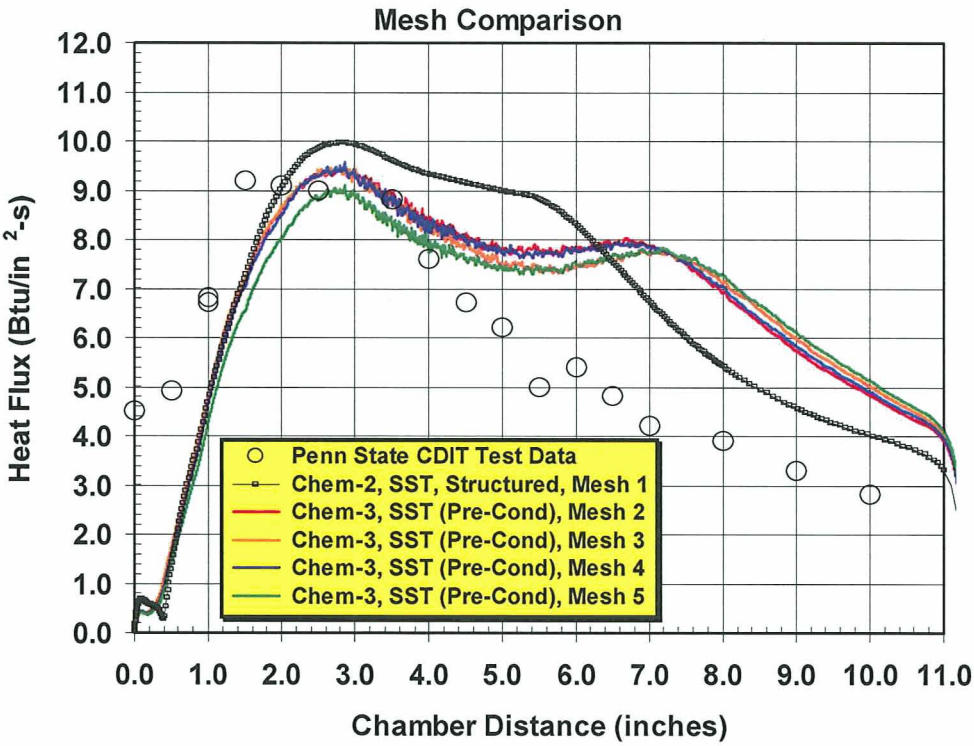

Figure 15. Comparison of predicted heat flux for the series of grides refining non-boundary layer portion of the computational domain.

Refinement of the boundary layer region is represented in Grids 6, 7 and 8. The range of the chamber wall first cell y-plus values are shown in Figure 16. Clearly for all cases the first cell y-plus values are appropriately small. The effects of the various boundary layer refinements on the predicted heat flux are shown in Figure 17. The net effect of the boundary layer refinements is to increase the heat flux in the upstream portion of the chamber and slightly decrease the heat flux in the downstream portion of the chamber.

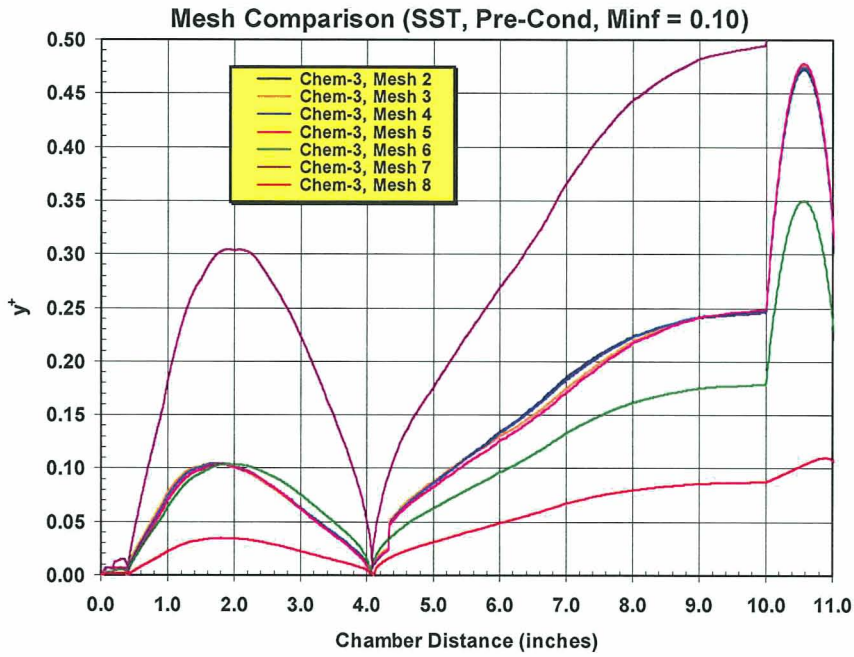

Figure16. Chamber wall first cell Y+ values for all hybrid grides.

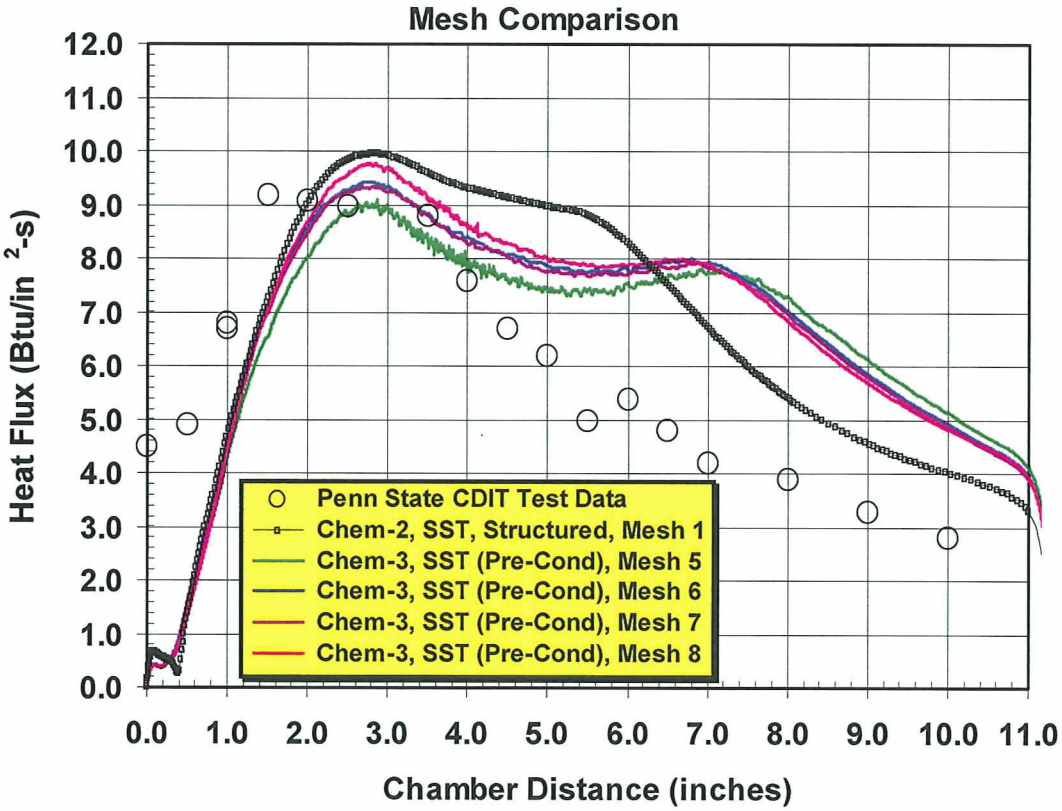

Figure 17. Comparison of predicted chamber wall heat fluxes for the series of grides used to assess boundary-layer region grid independence.

In terms of grid refinement, it is clear that the initial grid, Grid 2, is essentially an adequate grid for the prediction of chamber wall heat fluxes. The effects of the grid refinement in the non boundary-layer verse boundary layer are competing, but small. It is the opinion of the authors that in this progression of grides, that grid resolution effects have been driven down to the level that they are comparable to the effects of small changes in grid quality.

Conclusions

Conclusions can be drawn in three specific areas. The first is that in regards to the RCM-1 test case, the use or lack of use of preconditioning has no significant effect on the accuracy of the predicted chamber wall heat flux. However, the use of preconditioning does result in a significant increase in the efficiency of obtaining converged solutions to this test case when using the Loci-CHEM CFD program.

The second area is the sensitivity of the predicted heat transfer to the turbulence model chosen. The Menter Shear Stress Transport model provides superior performance, relative to the data in the upstream portion of the chamber, for the heat flux rise rate and peak value. This point is further amplified by the dissection of the computed solution which illustrates how the predicted twin peak nature of the heat flux arises from the distributions of the turbulent quantities relative to the velocity and thermal fields.

The last area is that reasonable grid independence has been demonstrated. The initial grid, Grid 2 with about 500,000 cells has been proven to be essentially providing the grid independent answer.

Overall, this effort demonstrates the limit of the predictive ability of the Loci-CHEM CFD program on the RCM-1 test case. Predictions of the initial heat flux rise rate and heat flux peak are satisfactory for engineering use. The heat flux is significantly over-predicted in the downstream portion of the chamber, rendering these predictions questionable for engineering use in this region.

Future Work

The mixed results found in this work illustrate the need to significantly improve the predictive ability of CFD methods. The demonstrated nature of the balances that lead the specific behavior of the heat flux prediction indicate that turbulence modeling should be addressed to achieve this improvement.

Improvements can be sought by investigating and improving RANS turbulence models, investing the use of LES methods and/or the use of hybrid RANS-LES methods. In any case, the evaluations should follow a very careful assessment of the proposed improvement via a hierarchy[12] of problems ranging from extremely simple and systematically progressing to more complex problems.

The grid refinement results presented in this paper can be further evaluated by applying advanced techniques[13] to the assessment of solution convergence. We will be pursuing these improvements in the future.

References

1 "Combustion Devices CFD Simulation Capability Roadmap", Tucker, P.K. and West, J., NASA/MSFC Fall Fluids Workshop, MSFC Alabama, November 21, 2002

2 "Guide for the verification and Validation of Computational Fluid Dynamics Simulations", AIAA G-077, 1998.

3 Herbert, S. and Luke, E. A., "Honey, I Shrunk the Grids! A New Approach to CFD Verification Studies", AIAA 2005-0685 , 44th Aerospace Sciences Meeting, January 9-12, 2006, Reno, NV.

4 Luke, E. A., Tong, X.-L. and Cinnella, P. "Numerical Simulations of Fluids with a General Equation of State", AIAA 2006-12951 44th Aerospace Sciences Meeting, January 9-12, 2006, Reno, NV.

5 Evans. J. S. and Schexnayder, C. J., "", AIAA Journal January 1980, Vol 18, No 2, p 188-193

6 Menter, F. R., "Two-Equation Eddy-Viscosity Turbulence Models for Engineering Applications," *AIAA Journal*, Vol. 32, No. 8, August 1994, pp. 1598–1605.

7 Wilcox, D. C., "Reassessment of the Scale-Determining Equation for Advanced Turbulence Models," *AIAA Journal*, Vol. 26, No. 11, 1988, pp. 1299–1310.

8 E. A. Luke and X-L. Tong and J. Wu and P. Cinnella "CHEM 2: A Finite-Rate Viscous Chemistry Solver -- The User Guide" MSSU-COE-ERC-04-07 Mississippi State University, September, 2004.

9 Luke, E. A., "A Rule-Based Specification System for Computational Fluid Dynamics", Ph.D. Dissertation, Mississippi State University, Starkville, MS, 1999

10 Gridgen, Software Package, Version 15, Pointwise, Inc., Bedford, Texas, 2005.

11 Santoro, R. J. and Lin, J. Y., "GO2/GH2 Injector Testing and Analysis" NASA/MSFC Spring Fluids Workshop, April 13-15, 2004.

12. Oberfampf, W. L., Trucano, T. G., and Hirsch, C., "Verification, Validation and predictive Capability in Computational Engineering and Physics," Sandia National Laboratories, Report SAND2003-3769, Albuquerque, NM, February, 2003

13. Roache, P. J., *Verification and Validation in Computational Science and Engineering*, Hermosa Publishers, Albuquerque, NM, 1998